ORIGINAL PAPER

Tin Oxide Thin Films

physica status solidi a

www.pss-a.com

Effects of Oxygen Ratio on the Properties of Tin Oxide Thin Films Doped with Bismuth

*Hyo In Bang, Han Byeol Seo, Byung Seong Bae, and Eui-Jung Yun**

This study examines the effects of the oxygen ratio on the properties of bismuth (Bi)-doped tin oxide (Bi-SnO_x) films deposited by radio frequency magnetron sputtering using a SnO (90 at%)-Bi (10 at%) ceramic target. The properties of the samples are characterized by X-ray photoelectron spectroscopy (XPS), Hall effect measurements, dynamic-secondary ion mass spectrometry (D-SIMS), and X-ray diffraction (XRD). The samples deposited without oxygen gas exhibit Sn^{4+} and Sn^{2+} XPS peak areas of 44.7 and 41.1%, respectively. The Sn^{4+} area increases to 64.1% with increasing oxygen ratio up to 20% with a concomitant decrease of the Sn^{2+} area to 26%, indicating that SnO_2 with n-type conductivity is the dominant phase under a higher oxygen partial pressure. XPS shows that with increasing oxygen ratio, the chemical state of Bi changes from metallic Bi (Bi^0) to Bi^{3+}. Furthermore, with increasing oxygen ratio, the Bi content in the samples increases because of the increase in Bi_2O_3 formation, which causes a decrease in the number of oxygen vacancies in the samples. These results suggest that the oxygen ratio is useful for controlling Bi doping in SnO_x films. Therefore, Bi doping is valuable for suppressing the formation of oxygen vacancies and improving the properties of SnO_x films.

1. Introduction

Transparent complementary metal oxide semiconductor (CMOS) circuits are an essential element to drive the microelectronics revolution. Their advantages over n-channel MOS (NMOS), such as low power dissipation and higher density of logic functions on a chip, can be realized if both high performance n- and p-type oxide thin-film transistors (TFTs) can be developed.[1–10] Therefore, the achievement of high performance n- and p-type oxide semiconductors (OSs) is an important issue for the development of giant microelectronics.

Tin oxide (SnO_x) thin films deposited by radio-frequency (RF) magnetron sputtering have been applied widely as the channel layer in the fabrication of flexible TFTs. This is because SnO_x films are n- and p-type OSs, inexpensive, chemically stable in strong acidic and basic solutions, thermally stable in oxidizing environments at high temperatures, and mechanically durable.[1–3,5–7,9–21] On the other hand, tin oxide has a relatively high carrier concentration, which makes TFTs difficult to turn OFF, and can be crystallized, which causes non-uniformity in the display.[20] These problems can be resolved by doping with suitable cations acting as carrier repressors and crystallization stoppers because tin oxide is a bipolar OS, in which both n- or p-type carrier doping are possible in the same SnO_x material. To date, several doping elements have been reported to improve the performance of tin-oxide-based TFTs, such as aluminum,[19,22] zirconium,[23,24] hafnium,[25] and fluorine.[26] Furthermore, lower valence cations, such as nitrogen (N),[27,28] indium,[28,29] and antimony (Sb),[28,29] have been suggested to be good p-type dopants in SnO_2. In contrast, SnO_2 films doped with bismuth (Bi),[20,30] which is a lower valence cation, N-doped SnO,[29] Sb-doped SnO_2 films,[31–33] and Sb-doped SnO_2 epitaxial films[34] exhibit n-type conductivity. Hence, there appears to be a discrepancy in the influences of lower valence cations on the properties of SnO_x thin films. Moreover, there are no reports showing the effects of Bi doping and sputtering process parameters on the properties of SnO_x films deposited using a SnO-Bi ceramic target. Therefore, this study examined the effects of the oxygen partial pressure on the properties of Bi-doped SnO_x thin films using a SnO (90 at%)-Bi (10 at%) ceramic target.

2. Results and Discussion

Figure 1 presents the SIMS depth profiles, exhibiting typical intensity variations in Sn, O, and Bi concentrations in the Bi-doped SnO_x thin films prepared at different oxygen ratios. As shown in Figure 1, the oxygen concentration was higher than

H. I. Bang, Prof. E.-J. Yun
Department of ICT Automotive Engineering
Hoseo University
Dangjin, Chungnam 31702, Republic of Korea
E-mail: ejyun@hoseo.edu

H. B. Seo
Department of NanoBio Tronics
Hoseo University
Asan, Chungnam 31499, Republic of Korea

Prof. B. S. Bae
Department of Display Engineering
Hoseo University
Asan, Chungnam 31499, Republic of Korea

The ORCID identification number(s) for the author(s) of this article can be found under https://doi.org/10.1002/pssa.201800863.

DOI: 10.1002/pssa.201800863

 © 2019 WILEY-VCH Verlag GmbH & Co. KGaA, Weinheim

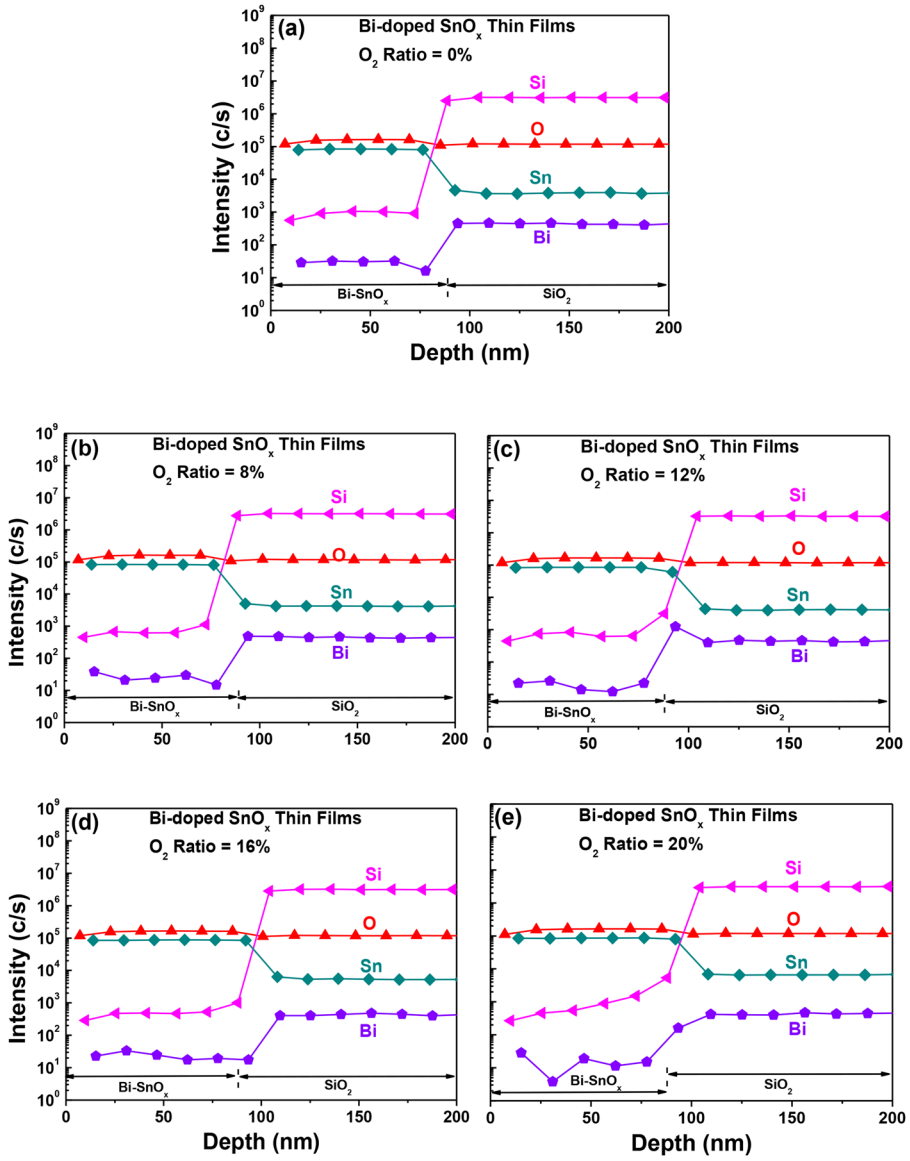

Figure 1. Intensity variations in the tin (Sn), oxygen (O), and bismuth (Bi) concentrations in the Bi-doped SnO_x thin films prepared at oxygen ratios of (a) 0, (b) 8, (c) 12, (d) 16, and (e) 20%, which were obtained from the SIMS depth profiles.

that of tin in all the prepared samples, suggesting that an oxygen rich phase, such as SnO_2, was dominant. Actually, we observed from the SIMS analyses (not shown) that the higher Ar working pressure was another factor to prepare more oxidized SnO_x films ($\approx SnO_2$). Therefore, we believe that in our case, the higher Ar working pressure caused the introduction of more oxygen atoms into the plasma in the chamber, which resulted in the more oxidized SnO_x films at even oxygen ratio of 0%. The Bi contents in the samples were smaller than those in the SiO_x substrate (Figure 1), which indicates that a smaller amount of Bi diffused into the SnO_x matrix compared to the SiO_x substrate. The low Bi density in the SnO_x films can be explained as follows. The electronegativity difference between Bi^{3+} (1.399) and O (3.758) is larger than that of Sn^{4+} (1.706) and O and that of Si^{4+} (1.887) and O.[35] The stronger binding of Bi to O makes it easier for Bi atoms to diffuse into the SnO_x and SiO_x films during the sputtering process. Furthermore, the stronger binding of Sn to O than that of Si to O makes it more difficult for Bi atoms to be introduced to SnO_x than SiO_x films. Therefore, the lower Bi density in the SnO_x films than that in SiO_x can be attributed to the larger electronegativity difference between Sn^{4+} and O than that of Si^{4+} and O, which causes stronger binding of Sn to O than that of Si to O. Here, the valence state of Bi should be +3 instead of +5 because the difference in electronegativity between Bi^{5+} (1.895) and O[35] is lower than that of Sn^{4+} and O and that of Si^{4+} and O, making it much more difficult for Bi atoms to diffuse into the SnO_x and SiO_x films. The scale of electronegativity for ions was determined through a linear regression equation which was taken from Li's work.[35] Six-coordinated radii were used because the ionic substances crystallize usually in the structures with coordination number of 6, as mentioned in ref. [35]. As shown in Figure 1, a smaller amount of Bi diffused into the SnO_x matrix

© 2019 WILEY-VCH Verlag GmbH & Co. KGaA, Weinheim

compared to the SiO_x substrate. This result cannot be justified by the concept of the ionic radii of Bi, Sn, and Si elements because the ionic radius of Si^{4+} (0.54 Å) was much shorter than that of Sn^{4+} (0.83 Å) and that of Bi^{3+} (1.17 Å),[36] which should cause the higher Bi density in the SnO_x films than that of SiO_x. This indicates that the concept of electronegativity of elements is more important than that of the ionic radii of elements in our system.

Figure 2 presents XRD patterns of Bi-doped SnO_x films deposited at various oxygen ratios. The adatom mobility and the reactions among Sn, Bi, and O are restricted on the unheated substrate surface during deposition, which induces a large number of defects in the Bi-doped SnO_x films. Therefore, very fine nanocrystalline or amorphous films are formed. As shown in Figure 2, all samples with different oxygen ratios of 0–20% showed a broad halo peak centered at ≈30.3° 2θ, which was assigned to a SnO_2 phase.[2,8–10,19] Figure 2 also showed that the small sharp peaks of SnO (101) and SnO (112) at 28.6 and 51.3° 2θ, respectively, observed in the sample with an oxygen ratio of 0% weakened and disappeared with increasing oxygen ratio.[2,8–10,19,37,38] This suggests that the main n-type SnO_2 and minor p-type SnO phases coexist in the sample with an oxygen ratio of 0% and the concentration of SnO phase decreases with increasing oxygen ratio, which causes the growth of the SnO_2 phase with increasing oxygen ratio. All the SnO, SnO_2, and Si diffraction peaks in Figure 2 were indexed using JCPDS cards # 06–0395, # 41–1445, and # 27–1402, respectively. XRD showed that an increase in Bi content, which results from the increase in oxygen ratio (see **Table 1**), enhances the formation of an amorphous phase in the films. This is agreement with the fact that doping with Bi results in uncrystallized simple binary oxides, such as ZnO, SnO_2, and In_2O_3.[20] If we consider the ionic radii of the elements, the diffusion of Bi with a longer radius (1.17 Å) into SnO_x, ZnO, and In_2O_3, which are binary oxides with shorter ionic radii of Sn^{4+} (0.83 Å), Zn^{2+} (0.88 Å), and In^{3+} (0.94 Å),[36] will cause the enhancement of degree of disorder in the oxide matrices, which in turn results in uncrystallized binary oxides.

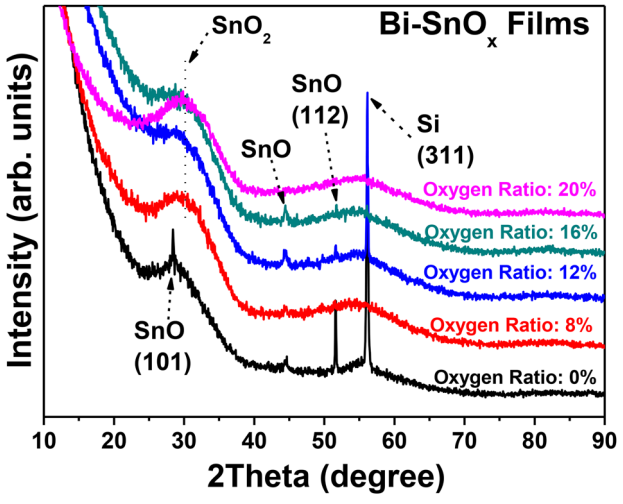

Figure 2. X-ray diffraction (XRD) patterns of Bi-doped SnO_x films deposited at various oxygen ratios.

Table 1. Summary of the contents (at%) of Bi, Sn, and O in the Bi-doped SnO_x films prepared at different oxygen ratios, which were analyzed by XPS.

Oxygen ratio of samples [%]	Bi [at%]	O [at%]	Sn [at%]
0	2.37	66.73	30.89
12	2.56	68.66	28.78
16	2.80	68.90	28.30
20	3.06	68.78	28.16

Table 1 lists the contents (at%) of Bi, Sn, and O in the Bi-doped SnO_x films prepared at different oxygen ratios, as determined by XPS. As listed in Table 1, the O and Bi contents increased with increasing oxygen ratio owing to the in-diffusion of O and Bi into the samples. Table 1 also confirmed the SIMS and XRD results in that an oxygen rich SnO_2 phase was dominant in the samples. Therefore, the larger oxygen content enhances the annihilation of oxygen vacancy (V_o) donor defects in the films, which in turn results in the decrease in the electronic density in the films. The larger Bi content also decreases the electron concentration in the samples. This can be explained by the larger electronegativity difference of Bi and O than that of Sn and O making it easier for Bi atoms to occupy the Sn sites due to the stronger binding of Bi to O than that of Sn to O. When Bi^{3+} substitutes Sn^{4+} in the crystal lattice of SnO_2 (the dominant phase in the sample according the XPS results in Table 1), the three valence electrons of Bi form covalent bonds with three of the Sn neighbors but the bond with the fourth neighbor remains unsatisfied. Then, Bi^{3+} will act as a compensation center (p-type dopant) and hence, decreases the electronic density. Therefore, the larger Bi content causes a decrease in the electron concentration in the samples. This was confirmed by Hall effect measurements in that the samples with a larger Bi content had a lower electron concentration, as shown in **Table 2**.

Table 2 lists the Hall effect measurements, which revealed the electrical properties of a series of Bi-doped SnO_x films prepared with four oxygen ratios of 0, 12, 16, and 20%. The samples exhibited n-type conductivity, regardless of the oxygen ratio. As shown in Table 2, the mobility (μ) and electron carrier concentration (n) decreased with increasing oxygen ratio, resulting in an increased resistivity (ρ). This result followed the equation,

$$\rho = \frac{1}{nq\mu} \tag{1}$$

where q is the charge of an electron. The large decrease in μ with increasing oxygen ratio was attributed mainly to an improved carrier scattering with increasing the defect density. Note that the diffusion of O and Bi into the Bi-doped SnO_x films produced in-band gap defects and caused an increase in resistance.[20] This suggests that the higher resistance of Bi-doped SnO_x thin films prepared at larger oxygen concentrations is related to the introduction of a larger amount of O and Bi into the Bi-doped SnO_x thin films. The V_o sites in the SnO_x films can be occupied by introduced oxygen, resulting in a decrease in the number of V_o donor defects, which causes a decrease in electron concentration and an increase in resistance, as evidenced by Table 2.

© 2019 WILEY-VCH Verlag GmbH & Co. KGaA, Weinheim

Table 2. Summary of the Hall effect measurement results for a series of samples prepared at two oxygen ratios.

Sample description	Resistivity [Ω•cm]	Hall mobility [$cm^2 V^{-1} s^{-1}$]	Electron carrier concentration [cm^{-3}]
Bi-doped SnO_x thin films deposited with an oxygen ratio of 0%	2.08	9.94	3.02×10^{17}
Bi-doped SnO_x thin films deposited with an oxygen ratio of 12%	8.92	6.73	1.04×10^{17}
Bi-doped SnO_x thin films deposited with an oxygen ratio of 16%	104	3.97	1.51×10^{16}
Bi-doped SnO_x thin films deposited with an oxygen ratio of 20%	Immeasurable owing to very high resistance		

All XPS binding energies were calibrated using the carbon (C) 1s reference peak centered at 284.6 eV. Two Sn 3d narrow-scan XPS peaks for the Bi-doped SnO_x thin films were detected at binding energies of 486.3 and 494.7 eV, which correspond to the spin orbit of Sn $3d_{5/2}$ and Sn $3d_{3/2}$, respectively.[2,8,9,16,17,19,20,39] The Sn $3d_{5/2}$ narrow-scan XPS spectra of the Bi-doped SnO_x thin films were fitted using three Gaussian peaks (GPs) related to the Sn^0, Sn^{2+}, and Sn^{4+} peaks centered at approximately 485.3–485.6, 486–486.3, and 486.5–486.8 eV, respectively, which correspond to metallic Sn, p-type SnO, and n-type SnO_2.

Figure 3a,b present typical examples of the Sn $3d_{5/2}$ narrow-scan XPS spectra fitted using three GPs in the Bi-doped SnO_x films prepared at different oxygen ratios of 0 and 20%, respectively. The fitting of the Sn $3d_{5/2}$ peaks using three GPs was excellent. As shown in Figure 3a, for the Bi-doped SnO_x films prepared at an oxygen ratio of 0%, the percentage areas of the Sn^0 peaks centered at 485.6 eV, Sn^{2+} peaks at 486.1 eV, and Sn^{4+} peaks at 486.6 eV were 14.2, 41.1, and 44.7%, respectively. Figure 3b also shows that the percentage areas of the Sn^0 peaks centered at 485.5 eV, Sn^{2+} peaks at 486.1 eV, and Sn^{4+} peaks at 486.7 eV were 9.9, 26.0, and 64.1%, respectively, for the Bi-doped SnO_x thin films prepared at an oxygen ratio of 20%.

Figure 4 shows the percentage areas of the three GPs as a function of the oxygen ratio for the Bi-doped SnO_x films prepared at various oxygen gas ratios, which were obtained after fitting the Sn $3d_{5/2}$ peaks using the three Sn^0, Sn^{2+}, and Sn^{4+} GPs, as shown several examples in Figure 3. As shown in Figure 4, the Sn^{4+} and Sn^{2+} XPS peak area percentages were 44.7 and 41.1%, respectively, for the Bi-doped SnO_x films prepared with an oxygen ratio of 0%, which indicates that there is a larger amount of SnO_2 phase in the sample than SnO. This is in good agreement with the SIMS result shown in Figure 1. The Sn^{4+} and Sn^{2+} peak area percentages increased and decreased, respectively, with increasing oxygen ratio. This is related to an increase in the concentration of Sn^{4+} ions due to the introduction of more O and Bi during deposition, as evident in Table 1. This is in agreement with recent reports showing that an increase in the amount of O within the SnO_x films results in an increase in the number of Sn^{4+} ions.[40] Figure 4 also shows that n-type SnO_2 was the main composition regardless of the change in oxygen ratio, as confirmed by Figures 1 and 2, and Table 2.

The O 1s narrow-scan XPS spectra of the Bi-doped SnO_x thin films were also fitted using three GPs related to the low, middle, and high peaks (LP, MP, and HP) centered at approximately 530.0–530.2, 530.5–531.2, and 531.7–531.8 eV, respectively. The LP was assigned to O^{2-} ions surrounded by Sn, Bi, and O atoms in a fully oxidized stoichiometric Bi-doped SnO_x system. The MP was also associated with O^{2-} ions in the oxygen-deficient regions within the Bi-doped SnO_x matrix and was related to V_o defects, whereas HP was related to chemisorbed or dissociated oxygen or to O-H bonding near the film surface.[41–44]

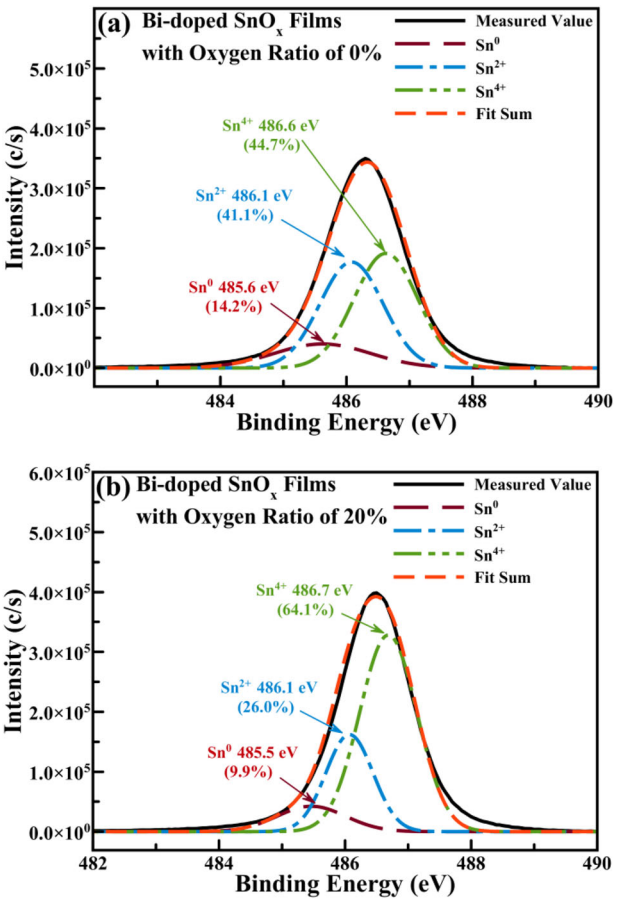

Figure 3. Typical Sn $3d_{5/2}$ narrow-scan XPS spectra fitted using three Gaussian peaks for the Bi-doped SnO_x thin films prepared at oxygen ratios of (a) 0 and (b) 20%.

© 2019 WILEY-VCH Verlag GmbH & Co. KGaA, Weinheim

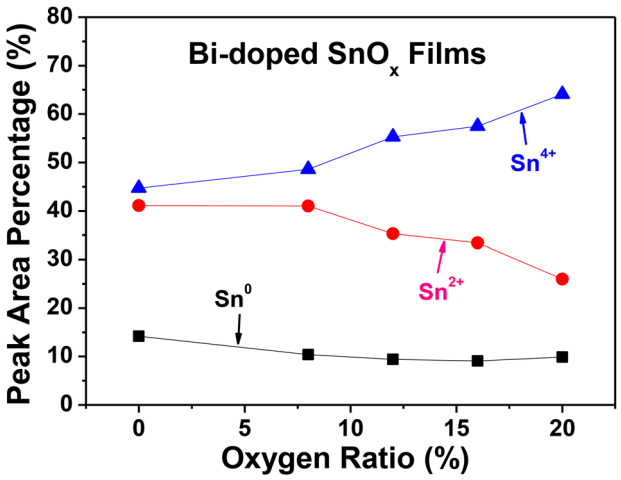

Figure 4. Percentage area characteristics of three Gaussian peaks as a function of the oxygen ratio obtained from the Sn $3d_{5/2}$ narrow scan XPS spectra of Bi-doped SnO_x thin films prepared at various oxygen ratios. This result was obtained after fitting the $3d_{5/2}$ peaks using the three Sn^0, Sn^{2+}, and Sn^{4+} Gaussian peaks, as shown in Figure 3.

Figure 5 presents the percentage areas of the three GPs as a function of the oxygen ratio for the samples prepared at various oxygen ratios, which were obtained after fitting the O 1s peaks using the three LP, MP, and HP GPs. In the case of the samples with oxygen ratios of 0–12%, the LP and MP areas increased and decreased, respectively, with increasing oxygen ratio. The decrease in MP area can be explained by the following argument. When Bi-doped SnO_x thin films were prepared at oxygen ratios of 0–12%, the in-diffusion of O from the chamber into the film increased significantly with increasing oxygen ratio, as evidenced by Table 1, resulting in the annihilation of oxygen vacancies (V_o) in the films, which caused a decrease in the number of V_o. The increase in LP area for the samples with oxygen ratios of 0–12% was also attributed to the enhancement of the reaction of Sn and Bi metals with O due to in-diffused O and Bi, as confirmed by Table 1. On the other hand, for the samples with oxygen ratios greater than 12%, the increase in the LP area and the decrease in the MP area decreased with increasing oxygen ratio, which suggests that the in-diffusion of O to the sample surface is reduced during sample deposition, as shown in Table 1. On the other hand, the HP area decreased slightly from 16.8 to 13.3% with increasing oxygen ratio (Figure 5). This suggests that the amount of O or H, which appeared near the surfaces of the Bi-doped SnO_x thin films, decreased marginally with increasing oxygen ratio, resulting from a decrease in the number of defects on the film surface due to in-diffused O and Bi.

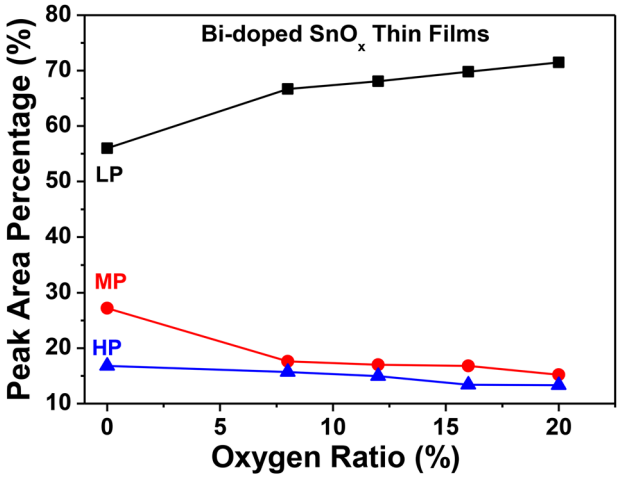

Figure 5. Percentage area characteristics of three Gaussian peaks as a function of the oxygen ratio obtained from the O1s narrow scan XPS spectra of Bi-doped SnOx thin films prepared at various oxygen ratios. This result was obtained after fitting the O 1s peaks using the three LP, MP, and HP Gaussian peaks.

To determine if the valence state of Bi in the samples is +3 or +5, **Figure 6** plots the Bi 4f region of XPS spectra of Bi-doped SnO_x thin films with different oxygen ratios. The broad and asymmetric Bi 4f peaks confirmed the existence of Bi in the samples. For the samples with an oxygen ratio of 0%, the four Bi peaks appeared as follows: two Bi $4f_{7/2}$ core levels at 156.96 and 159.43 eV, and two Bi $4f_{5/2}$ core levels at 162.31 and 164.67 eV. The two peaks centered at 156.96 eV (Bi $4f_{7/2}$) and 162.31 eV (Bi $4f_{5/2}$) were assigned to the zero valence or metallic state of Bi (Bi^0), whereas the other two peaks at 159.43 eV (Bi $4f_{7/2}$) and 164.67 eV (Bi $4f_{5/2}$) were attributed to the three valence states of Bi (Bi^{3+}). These Bi peak positions are in good agreement with the data obtained using the (Al/)Mg laboratory XPS source.[20,45–47] As the Bi content was increased, which results from an increase in oxygen ratio (see Table 1), the intensity of the Bi^{3+} peaks increased sharply, whereas that of metallic Bi^0 peaks almost vanished. This suggests that the Bi ions in the Bi-doped SnO_x films are in the chemical state of Bi^{3+} rather than Bi^{5+}, which confirms the aforementioned argument in Figure 1. Therefore, this study provides strong evidence for the variation of the chemical state of bismuth in the Bi-doped SnO_x films.

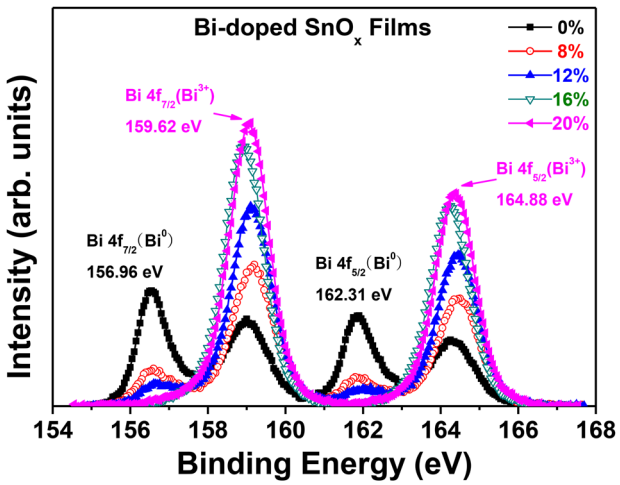

Figure 6. Variation of Bi 4f narrow-scan XPS spectra for the Bi-doped SnO_x thin films prepared at different oxygen ratios of 0–20%.

© 2019 WILEY-VCH Verlag GmbH & Co. KGaA, Weinheim

3. Conclusion

This study examined the effects of the oxygen partial pressure on the properties of Bi-doped SnO_x thin films using a SnO (90 at %)-Bi (10 at%) ceramic target. All experimental results confirmed that an oxygen-rich n-type SnO_2 phase was dominant in the samples. In addition, an increase in Bi contents, which arises from an increase in the oxygen ratio, enhanced the formation of an amorphous phase in the films. Hall effect measurements showed that the samples with a larger Bi content had a lower electron concentration and higher resistance, which are related to the introduction of a larger amount of O and Bi into the samples. As the oxygen ratio was increased, more O and Bi were introduced, which induced an increase in the concentration of Sn^{4+} ions and a decrease in the number of Sn^{2+} ions. The increased in-diffusion of O from the chamber into the films with increasing oxygen ratio resulted in a decrease in the number of oxygen vacancies. The experimental result clearly suggests that the Bi ions in the Bi-doped SnO_x films are in the chemical state of Bi^{3+} rather than Bi^{5+}. Therefore, this study provides strong evidence for the variation of the chemical state of bismuth in Bi-doped SnO_x films.

4. Experimental Section

SnO_x thin films were deposited on 300-nm-thick SiO_2 coated 400-μm-thick Si or eagle glass substrates at room temperature (RT) using a SnO (90 atomic %)-Bi (10 atomic %) mixed ceramic target (99.999%, 2 inch diameter) under the following conditions: radio frequency (RF) power of 50 W, working pressure of 0.667 Pa, and oxygen ratios $\left(=\frac{\text{oxygen}}{\text{argon}+\text{oxygen}}\times 100\right)$ of 0, 8, 12, 16, and 20%. Pure argon (99.999%) and oxygen gas mixtures were used as the reaction gas and the total flow rate was 25 sccm. The substrate-to-target distance and deposition time were kept constant at 10 cm and 30 min., respectively, for all depositions. The substrate was rotated at 13 rpm to deposit the SnO_x thin films with a uniform thickness. The SnO_x film thickness was approximately 88.4 nm.

The contents (at%) and chemical bonding states of Bi, Sn, and O in the Bi-doped SnO_x thin films were analyzed by X-ray photoelectron spectroscopy (XPS). The changes in the depth profiles of Bi, Sn, and O in the samples were examined by dynamic secondary ion mass spectrometry (D-SIMS). The electrical properties of the SnO_x thin films were measured at RT using a Hall effect measurement system according to a van der Pauw configuration after forming the Ohmic contacts with a 100-nm-thick Al layer using a sputtering system, followed by alloying at 150 °C in air for 1 h. The structures of the films were characterized by X-ray diffraction (XRD) using a Cu $K\alpha_1$ radiation source ($\lambda = 0.15406$ nm).

Acknowledgement

This study was supported by the Basic Science Research Program through the National Research Foundation of Korea (NRF) funded by the Ministry of Education (NRF-2016R1D1A3B03932570).

Conflict of Interest

The authors declare no conflict of interest.

Keywords

bismuth doping, oxygen ratio, oxygen vacancies, SnO:Bi ceramic target, tin oxide (SnO) thin films

Received: November 12, 2018
Revised: December 29, 2018
Published online: January 22, 2019

[1] E. Fortunato, P. Barquinha, R. Martins, *Adv. Mater.* **2012**, *24*, 2945.
[2] L. Guo, M. Zhao, D. Zhuang, Q. Gong, H. Tan, M. Cao, L. Ouyang, *Mater. Sci. Semicond. Proc.* **2016**, *46*, 35.
[3] L. Qiang, W. Liu, Y. Pei, G. Wang, R. Yao, *Solid-State Electron.* **2017**, *129*, 163.
[4] R. Martins, A. Nathan, R. Barros, L. Pereira, P. Barquinha, N. Correia, R. Costa, A. Ahnood, I. Ferreira, E. Fortunato, *Adv. Mater.* **2011**, *23*, 4491.
[5] C. Ju, C. Park, H. Yang, U. Kim, Y. M. Kim, K. Char, *Curr. Appl. Phys.* **2016**, *16*, 300.
[6] J.-H. Lee, Y.-J. Choi, C.-Y. Jeong, D.-K. Jung, S. Ham, H.-I. Kwon, *IEEE Electron Dev. Lett.* **2016**, *37*, 300.
[7] A. Azmi, J. Lee, T. J. Gim, R. Choi, J. K. Jeong, *IEEE Electron Dev. Lett.* **2017**, *38*, 1543.
[8] P.-C. Chen, Y.-C. Chiu, Z.-W. Zheng, C.-H. Cheng, Y.-H. Wu, *J. Alloys Compd.* **2017**, *707*, 162.
[9] H. Luo, L. Liang, H. Cao, *Solid-State Electron.* **2017**, *129*, 88.
[10] J. S. Ahn, R. Pode, K. B. Lee, *Thin Solid Films* **2016**, *608*, 102.
[11] Y. Ogo, H. Hiramatsu, K. Nomura, H. Yanagi, T. Kamiya, M. Hirano, H. Hosono, *Appl. Phys. Lett.* **2008**, *93*, 032113.
[12] L. Y. Liang, Z. M. Liu, H. T. Cao, Z. Yu, Y. Y. Shi, A. H. Chen, H. Z. Zhang, Y. Q. Fang, X. L. Sun, *J. Electrochem. Soc.* **2010**, *157*, H598.
[13] J. Um, B. M. Roh, S. Kim, S. E. Kim, *Mater. Sci. Semicond. Proc.* **2013**, *16*, 1679.
[14] P. C. Hsu, W. C. Chen, Y. T. Tsai, Y. C. Kung, C. H. Chang, C. J. Hsu, C. C. Wu, H. H. Hsieh, *Jpn. J. Appl. Phys.* **2013**, *52*, 05DC07.
[15] P. C. Hsu, W. C. Chen, Y. T. Tsai, Y. C. Kung, C. H. Chang, C. C. Wu, H. H. Hsieh, *Thin Solid Films* **2014**, *555*, 57.
[16] S.-S. Lin, Y.-S. Tsai, K.-R. Bai, *Appl. Surf. Sci.* **2016**, *380*, 203.
[17] S.-S. Lin, S.-Y. Fan, Y.-S. Tsai, *Ceram. Int.* **2017**, *43*, 1802.
[18] H.-J. Kim, C.-Y. Jeong, S.-D. Bae, J.-H. Lee, H.-I. Kwon, *IEEE Electron Dev. Lett.* **2017**, *38*, 473.
[19] A. H.-T. Nguyen, M.-C. Nguyen, J. Choi, S. Han, J. Kim, R. Choi, *Thin Solid Films* **2017**, *641*, 24.
[20] J. Yang, S. Pi, Y. Han, R. Fu, T. Meng, Q. Zhang, *IEEE Trans. Electron Devices* **2016**, *63*, 1904.
[21] B. L. Zhu, X. Zhao, W. C. Hu, T. T. Li, J. Wu, Z. H. Gan, J. Liu, D. W. Zeng, C. S. Xie, *J. Alloys Compd.* **2017**, *719*, 429.
[22] M. S. Huh, B. S. Yang, S. Oh, J. Lee, K. Yoon, J. K. Jeong, C. S. Hwang, H. J. Kim, *Electrochem. Solid-State Lett.* **2009**, *12*, H385.
[23] D.-S. Han, J.-H. Park, Y.-J. Kang, J.-W. Park, *Microelectron. Rel.* **2013**, *53*, 1875.
[24] X. Zhang, X. Liu, H. Ning, W. Yuan, Y. Deng, X. Zhang, S. Wang, J. Wang, R. Yao, J. Peng, *Superlattices Microstruct.* **2018**, *123*, 330.
[25] W.-S. Kim, Y.-K. Moon, K.-T. Kim, S.-Y. Shin, J.-W. Park, *Thin Solid Films* **2012**, *520*, 2220.
[26] B. L. Zhu, F. Liu, K. Li, K. Lv, J. Wu, Z. H. Gan, J. Liu, D. W. Zeng, C. S. Xie, *Ceram. Int.* **2017**, *43*, 10288.
[27] S. S. Pan, G. H. Li, L. B. Wang, Y. D. Shen, Y. Wang, T. Mei, X. Hu, *Appl. Phys. Lett.* **2009**, *95*, 222112.
[28] Y. Kim, J. H. Jang, J. S. Kim, S. D. Kim, S. E. Kim, *Mater. Sci. Eng. B* **2012**, *177*, 1470.
[29] Y. Kim, J. Um, S. Kim, S. E. Kim, *ECS Solid State Lett.* **2012**, *1*, 29.
[30] C. Z. Chen, S. W. Zhu, W. Q. Zhang, Y. Li, C. B. Cai, *Results Phys.* **2017**, *7*, 2588.

© 2019 WILEY-VCH Verlag GmbH & Co. KGaA, Weinheim

[31] A. Ammari, M. Trari, B. Bellal, N. Zebbar, *J. Electroanal. Chem*. **2018**, *823*, 638.
[32] E. Elangovan, K. Ramamurthi, *Cryst. Res. Technol*. **2003**, *38*, 779.
[33] A. Ammari, M. Trari, N. Zebbar, *Mater. Sci. in Semicond. Proc*. **2019**, *89*, 97.
[34] C. Luan, Z. Zhu, W. Mi, J. Ma, *J. Alloys Compd*. **2014**, *586*, 426.
[35] K. Li, D. Xue, *J. Phys. Chem. A* **2006**, *110*, 11332.
[36] R. D. Shannon, *Acta Crystallogr. A* **1976**, *32*, 751.
[37] L. Y. Liang, Z. M. Liu, H. T. Cao, X. Q. Pan, *ACS Appl. Mater. Inferfaces* **2010**, *2*, 1060.
[38] X. Chu, X. Zhu, Y. Dong, W. Zhang, L. Bai, *J. Mater. Sci. Technol*. **2015**, *31*, 913.
[39] D. M. Priyadarshini, R. Mannam, M. S. R. Rao, N. DasGupta, *Appl. Surf. Sci*. **2017**, *418*, 414.
[40] H. Luo, L. Y. Liang, H. T. Cao, M. Z. Dai, Y. C. Lu, M. Wang, *ACS Appl. Mater. Interfaces* **2015**, *7*, 17023.
[41] C.-H. Hung, S.-J. Wang, P.-Y. Liu, C.-H. Wu, H.-P. Yan, N.-S. Wu, T.-H. Lin, *Mater. Sci. Semicond. Proc*. **2017**, *67*, 84.
[42] H. Xie, J. Xu, G. Liu, L. Zhang, C. Dong, *Mater. Sci. Semicond. Proc*. **2017**, *64*, 1.
[43] M.-H. Kim, M.-J. Choi, K. Kimura, H. Kobayashi, D.-K. Choi, *Solid-State Electron*. **2016**, *126*, 87.
[44] Y.-H. Joo, C.-I. Kim, *Thin Solid Films* **2015**, *583*, 40.
[45] R. Schafranek, J. D. Baniecki, M. Ishii, Y. Kotaka, K. Kurihara, *New J. Phys*. **2013**, *15*, 053014.
[46] K. Jiang, J. J. Zhu, J. D. Wu, J. Sun, Z. G. Hu, J. H. Chu, *ACS Appl. Mater. Interfaces* **2011**, *3*, 4844.
[47] S. Chaturvedi, I. Sarkar, M. M. Shirolkar, U.-S. Jeng, Y.-Q. Yeh, R. Rajendra, N. Ballav, S. Kulkarni, *Appl. Phys. Lett*. **2014**, *105*, 102910.

© 2019 WILEY-VCH Verlag GmbH & Co. KGaA, Weinheim